Applied Physics Letters

Wide wavelength-tunable narrow-band thermal radiation from moiré patterns

Cite as: Appl. Phys. Lett. **118**, 131111 (2021); https://doi.org/10.1063/5.0047308
Submitted: 12 February 2021 • Accepted: 02 March 2021 • Published Online: 31 March 2021

Cheng Guo, Yu Guo, Beicheng Lou, et al.

Applied Physics Letters ARTICLE scitation.org/journal/apl

Wide wavelength-tunable narrow-band thermal radiation from moiré patterns

Cite as: Appl. Phys. Lett. **118**, 131111 (2021); doi: 10.1063/5.0047308
Submitted: 12 February 2021 · Accepted: 2 March 2021 ·
Published Online: 31 March 2021

View Online Export Citation CrossMark

Cheng Guo,[1] Yu Guo,[2] Beicheng Lou,[1] and Shanhui Fan[2,a)]

AFFILIATIONS

[1]Department of Applied Physics, Stanford University, Stanford, California 94305, USA
[2]Ginzton Laboratory and Department of Electrical Engineering, Stanford University, Stanford, California 94305, USA

[a)]Author to whom correspondence should be addressed: shanhui@stanford.edu

ABSTRACT

Wavelength-tunable narrow-band thermal emitters are highly desired for various applications including multigas sensing. However, current thermal emitters suffer from either too broad bandwidth or too narrow tuning range. Here, based on the moiré effect, we provide a scheme of wavelength-tunable narrow-band thermal emitters with tunability over a wide wavelength range and operation at an arbitrary temperature. Thanks to the unique sensitivity of moiré patterns, our emitter achieves a tuning range to bandwidth ratio of 313, which is 68 times larger than the previous largest value ever reported.

Thermal absorption and emission are linked through Kirchhoff's law. Conventional thermal absorbers provide broadband absorption, and conventional thermal emitters generate broadband and incoherent thermal radiation.[1,2] Moreover, the tunability of most conventional structures is limited. However, wavelength-tunable narrowband thermal emitters and absorbers are desired in many applications including gas sensing[3–5] and infrared imaging,[6] and in many devices including microbolometers[7,8] and pyroelectric detectors.[4] One important example is non-dispersive infrared (NDIR) sensing, which detects the concentration of target gases based on their characteristic infrared absorption.[3–5] In conventional NDIR sensors, broadband thermal light sources are used. To select the target gas, a bandpass filter has to be added before the detector. Hence, to analyze multiple target gases in a mixture simultaneously, multiple pairs of bandpass filters and detectors are required.[9,10] Such a scheme of multiplexed NDIR gas sensing is bulky, expensive, and complicated, especially when the number of target gases is large or their absorption features overlap.[11] This challenge is fundamentally rooted in the lack of cost-effective tunable narrow-band infrared light sources that cover a wide range of wavelengths.[4] Furthermore, sensitive absorption detection desires high spectral brightness and spatial coherence of the light source.

Despite significant previous effort,[2,12–19] it remains challenging to achieve a narrow-band and wavelength-tunable thermal emitter with tunability over a wide range of wavelengths. One approach to create a tunable thermal emitter is to integrate multiple different-wavelength narrow-band thermal emitters on a single device and to switch between these devices.[11,15] However, the switchable wavelengths are limited by the number of integrated emitters. Moreover, at any given time, only part of the device area is used, which limits the total power output. Another approach is to construct thermal emitters using thermochromic materials such as $Ge_2Sb_2Te_5$ (GST),[16,20,21] VO_2,[13] and Ge.[22] However, this approach can only offer tunability when operating within a specific temperature range since the dielectric properties of these materials are usually sensitive to temperature variation only within such a range.

As one measures the performance of tunable narrow-band thermal emitters, we define a figure of merit $F = \Delta\lambda_t/\Delta\lambda_b$, where $\Delta\lambda_t$ is its tuning range and $\Delta\lambda_b$ is the bandwidth of its thermal emission peak. In the context of gas sensing, a larger figure of merit indicates that the emitter can produce a larger number of independent spectra. The largest figure of merit ever reported is $F = 27.1\,\text{nm}/5.9\,\text{nm} = 4.6$.[22]

In this work, we propose a scheme to realize a wide-tunable narrow-band thermal emitter based on the geometric moiré effect. The figure of merit of our design far exceeds previous works. As shown in Fig. 1, the structure consists of two dielectric gratings separated from a flat metallic surface by a vacuum gap. The two dielectric gratings have different periods and are relatively rotated by an angle α. The superposition of these two gratings forms a moiré pattern creating a two-dimensionally periodic structure, of which the period is strongly α-dependent. The emissivity spectra exhibit sharp peaks corresponding to the guided resonances of the two-dimensionally periodic

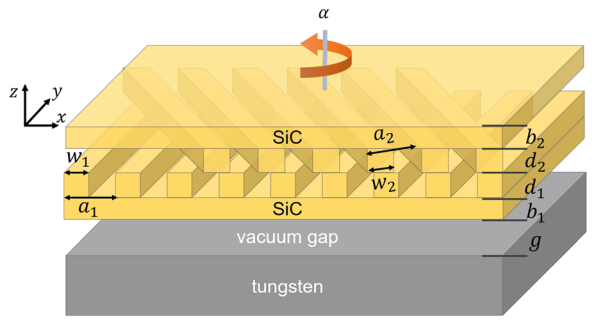

FIG. 1. Schematic of the tunable thermal emitter structure. The structure consists of two dielectric gratings made of SiC separated from a flat tungsten surface by a vacuum gap. The two line gratings exhibit different one-dimensional periods a_1 and a_2, respectively, and the top one is twisted with respect to the bottom one counterclockwise by an angle α. The superposition of these two gratings forms a moiré pattern with an α-dependent period. The structure parameters are $g = 0.26\,\mu$m, $b_1 = 0.125\,\mu$m, $d_1 = 0.15\,\mu$m, $d_2 = 0.15\,\mu$m, $b_2 = 0.125\,\mu$m, $a_1 = \frac{1}{6}\,\mu$m, $w_1 = \frac{1}{12}\,\mu$m, $a_2 = \frac{1}{5}\,\mu$m, $w_2 = \frac{1}{10}\,\mu$m.

structure. The peak wavelengths can be tuned continuously over a broad range by varying α. The giant tunablity results from the unique high sensitivity of moiré patterns to the small variation of the overlaid structures. The relative rotation can be readily implemented using the mature MEMS techniques.[23]

To discuss the underlying physics of our proposal, we start by briefly reviewing the thermal emission from a structure consisting of a single grating separated from a lossy metal surface by a vacuum gap, as discussed in Ref. 24. For concreteness, we consider SiC as the dielectric and W as the metal. In the energy range of 0.4– 1.4eV, the dielectric constant of SiC varies between 6.5 and 6.6, and its loss is negligible.[25] The thermal emission, thus, arises from the material loss of W. We plot the four lowest order guided modes of a uniform SiC slab with a thickness of 0.40 μm in Fig. 2(a). When periodic patterns are introduced to the slab, some of these guided modes become guided resonances that can couple to free space.[26] By placing the patterned slab near a flat metallic surface, the whole structure can exhibit narrow-band thermal emissivity thanks to the guided resonances.[24] As an illustration, we consider a structure where the grating has a lattice constant of $a = 0.8\,\mu$m, a grating width of $w = 0.4\,\mu$m, a grating depth of $d = 0.02\,\mu$m, and a base thickness of $b = 0.39\,\mu$m. The effective thickness of the slab is, thus, $(b + d/2) = 0.40\,\mu$m. The vacuum gap between the bottom of the grating and the W surface has a size of $g = 0.18\,\mu$m. The gap size is chosen such that the intrinsic loss rates of the guided resonances are close to their external loss rates, so that the peak emissivity is high.[24] We calculate the thermal emission spectra from such a structure using the Fourier modal method.[27] Figure 2(b) plots the emissivity spectra in the normal direction for both S and P polarization. Both spectra exhibit narrow-band peaks superposed on a smooth broadband background. Due to the mirror symmetry, the emissivity peaks for S and P polarizations result from the TE- and TM-guided resonances, respectively. The peak linewidths are ultranarrow: for example, the lowest peak has a full width at half maximum (FWHM) of 0.002 eV, corresponding to a quality factor of $Q = 323$.

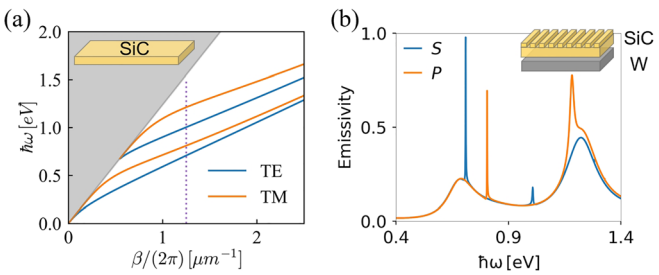

FIG. 2. Narrow-band thermal emission from guided resonances. (a) The lowest four guided modes of a uniform SiC slab with a thickness of $d = 0.40\,\mu$m. The inset shows the structure. The vertical dotted line corresponds to the lowest order reciprocal lattice vector of the grating in (b) and indicates the phase matching condition of the guided mode with a normally incident plane wave. (b) The thermal emission spectra from a single SiC grating with one-dimensional periodicity separated from a flat tungsten surface by a vacuum gap. The inset shows the structure. The structure parameters are the vacuum gap $g = 0.18\,\mu$m, the base thickness $b = 0.39\,\mu$m, the grating depth $d = 0.02\,\mu$m, the grating period $a = 0.8\,\mu$m, and the grating width $w = 0.4\,\mu$m.

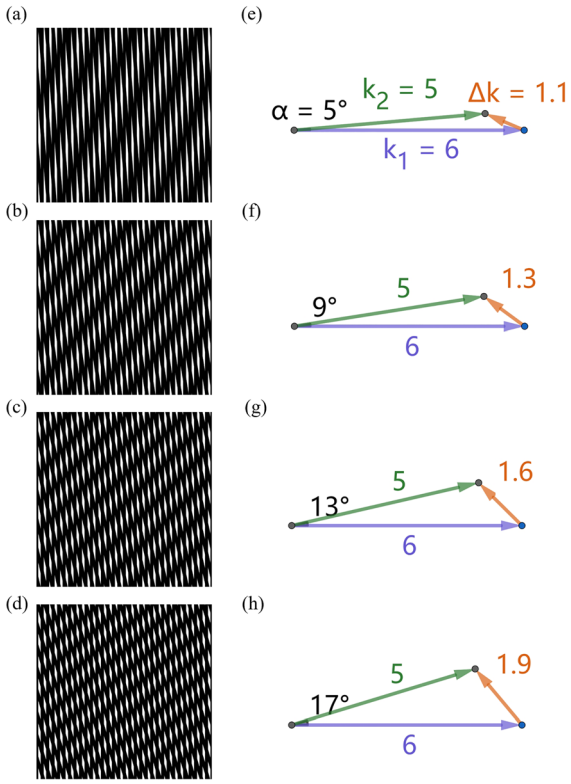

FIG. 3. Moiré patterns formed by the superposition of two line gratings. The first grating is periodic along the x-direction with a period of $a_1 = \frac{1}{6}\,\mu$m. The second grating has a period of $a_2 = \frac{1}{5}\,\mu$m and is rotated by an angle α counterclockwise with respect to the first grating. [(a)–(d)] The real space images of the Moiré patterns when $\alpha = 5°, 9°, 13°, 17°$. [(e)–(h)] The reciprocal space representation of the corresponding images. For clarity, we only draw the lowest order reciprocal lattice vectors. $\boldsymbol{k}_1$ and $\boldsymbol{k}_2$ are the reciprocal lattice vectors for the first and the second gratings, respectively. $\Delta\boldsymbol{k} = \boldsymbol{k}_1 - \boldsymbol{k}_2$ corresponds to the reciprocal lattice vector of the moiré fringes. The magnitudes of the reciprocal vectors are in unit $2\pi\,\mu m^{-1}$.

For a thermal emitter based on guided resonance, the peak frequencies can be varied by varying the grating period.[24] Here, we construct a grating with a tunable period utilizing the moiré effect. The moiré effect refers to the emergence of new patterns when repetitive structures are superposed on each other.[28] Recently, there has been significant interest in exploring moiré effects in photonics.[29–33] For concreteness, we consider the simple case of two binary square-wave gratings. The first grating is periodic along the x-direction with a period of $a_1 = \frac{1}{6}\ \mu$m and is constant along the y-direction. The second grating has a period of $a_2 = \frac{1}{5}\ \mu$m and is rotated by an angle α counterclockwise with respect to the first grating. The periodicities of both gratings are chosen to be deep subwavelengths so that each grating alone cannot support guided resonances in the wavelength range of interest. Figures 3(a)–3(d) show the superposition of the two line gratings in real space when $\alpha = 5°, 9°, 13°$, and $17°$. For visualization, we represent the dielectric and air as black and white, respectively. When the two gratings are stacked, clear moiré fringes appear. The apparent pale areas correspond to where the top dielectric (air) region is placed atop the bottom dielectric (air) region, while the apparent dark areas correspond to where the top dielectric (air) region is placed atop the bottom air (dielectric) region. The two-grating structure, thus, is a two-dimensional periodic structure. For a small rotation angle α as considered, the lowest order moiré fringes consist of alternating dark and pale lines that resemble an effective one-dimensional grating. Such moiré fringes exhibit much larger periodicity than both the underlying gratings so that they can support guided resonances in the wavelength range of interest. Moreover, the periodicity of the moiré fringes is strongly α-dependent and decreases significantly with the small increase in α.

To better understand the above moiré patterns, it is useful to investigate them in the reciprocal space. Figures 3(e)–3(h) show the reciprocal space representation of the corresponding images of Figs. 3(a)–3(d), respectively. For clarity, we only draw the lowest order reciprocal lattice vectors that dominate the spectral response. The purple arrow indicates the lowest order reciprocal lattice vector $\boldsymbol{k}_1$ of the first grating that is fixed, while the green arrow indicates the lowest order reciprocal lattice vector $\boldsymbol{k}_2$ of the second grating that is rotated. The angle between $\boldsymbol{k}_1$ and $\boldsymbol{k}_2$ is the same as the rotation angle α. The difference in the two reciprocal vectors $\Delta\boldsymbol{k} = \boldsymbol{k}_1 - \boldsymbol{k}_2$ (red arrow) corresponds to the reciprocal vector of the moiré fringes. Since the periods of both underlying gratings are deep subwavelengths and α is small, $|\Delta\boldsymbol{k}| < |\boldsymbol{k}_1|, |\boldsymbol{k}_2|$. As α increases, the magnitude of the moiré wavevector $|\Delta\boldsymbol{k}|$ increases and the moiré period $p = 2\pi/|\Delta\boldsymbol{k}|$ decreases.

Since the moiré patterns resemble an effective grating with tunable periodicity, they can be used to construct wavelength-tunable narrow-band thermal emitters. We consider the device as shown in Fig. 1. As discussed above, the guided resonances are induced exclusively from the lowest order moiré patterns in the wavelength range of interest. As the rotation angle α increases, the moiré wavevector magnitude $|\Delta\boldsymbol{k}|$ increases. Hence, the guided modes that are phase matched to the normal direction are blue-shifted, as depicted in Fig. 4(a). In Figs. 4(b)–4(e), we plot the emissivity spectra for x-polarized light in the normal direction when $\alpha = 5°, 9°, 13°$, and $17°$, respectively. These spectra are also calculated using a Fourier modal method.[27] As the relative rotation breaks the mirror symmetry, both TE and TM modes can couple to x-polarized light, leading to narrow emissivity peaks. As α increases, all these narrow peaks shift significantly to the higher frequency as expected. Here, we focus on the two lowest order modes. When $\alpha = 5°, 9°, 13°$, and $17°$, the resonant frequencies of the first mode are 0.720 eV, 0.852 eV, 1.015 eV, and 1.189 eV, respectively, while those of the second mode are 0.799 eV, 0.914 eV, 1.061 eV, and 1.239 eV, respectively. The linewidths of the resonances remain almost constant $\Delta\omega_b \approx 0.001\,5$ eV for both modes. Therefore, the figure of merit is

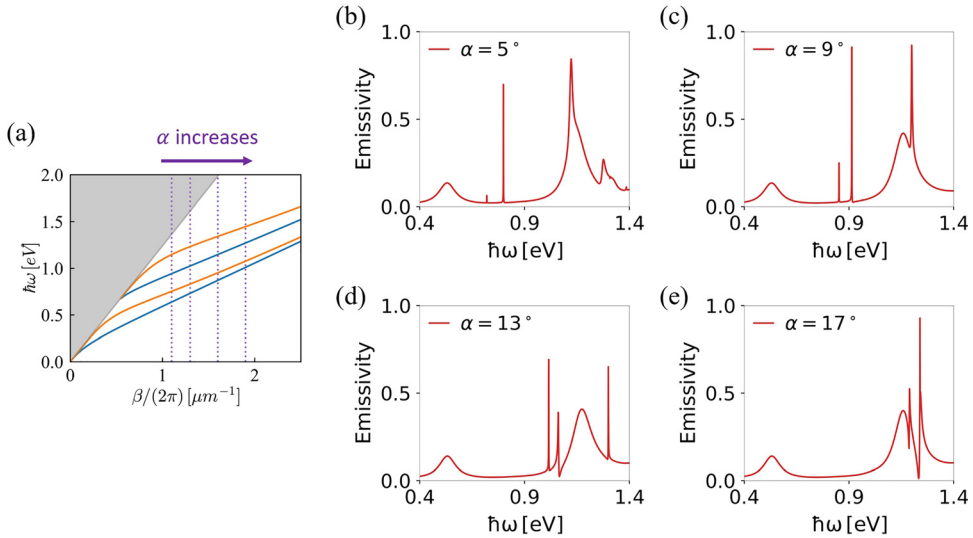

FIG. 4. Tunable narrow-band thermal emission from moiré patterns. The structure is shown in Fig. 1. (a) The guided modes that get phase matched to the normally incident plane waves are blue-shifted as α increases. The vertical dotted lines correspond to the moiré wavevector magnitude $|\Delta\boldsymbol{k}|$ and indicate the phase matching condition to the normal direction. (b)–(e) The emissivity spectra of the x-polarized wave when $\alpha = 5°, 9°, 13°$, and $17°$, respectively. The narrow emissivity peaks shift significantly with a small increase in α.

$F = \Delta\omega_t/\Delta\omega_b \approx 313$, which is 68 times larger than the previous largest ever reported value (4.6).[22] An even larger ratio can be achieved by considering larger rotation angles. Such giant tunability is crucial for applications like multigas sensing. We also note that the peak height varies as α varies due to the variation of the critical coupling condition.[24] The smooth background emissivity is low in the range of $0.5\text{eV} - 1.0\,\text{eV}$, which is advantageous for sensing applications.

Here, we make a few remarks. First, unlike the previous works using thermochromic materials, our approach is based on the pure geometric effects of moiré patterns. Therefore, it is not restricted to any specific material and allows for operation at an arbitrary temperature. Second, the relative rotation of the gratings can be readily implemented and accurately controlled with the current MEMS technologies.[23] Thanks to the unique sensitivity of moiré patterns, a small range of rotation angles is sufficient to achieve the giant wavelength tunability, which is advantageous for fast and efficient mechanical scanning. Third, although we consider a specific range of operating frequencies for concreteness, the same approach can be easily applied to other operating frequencies of interest. Fourth, the emissivity spectra have an angle dependence due to the band dispersion of the guided resonances. Such an angle dependence has been discussed in detail in Ref. 24. In this work, we have primarily focused on the emissivity in the normal direction. But similar tunability in thermal emission should be achievable in the off-normal direction as well. Finally, the tunable thermal emitter considered in this work is reciprocal and satisfies Kirchhoff's law. The same strategy can be readily extended to nonreciprocal thermal emitters to achieve tunable nonreciprocal thermal emission.[34–36] One possible realization is to use two twisted line gratings made of magnetic Weyl semimetals.[37–39]

In conclusion, we propose a wavelength-tunable narrow-band thermal emitter using dynamic moiré patterns. Thanks to the unique high sensitivity of moiré patterns, our emitter exhibits both an ultranarrow linewidth (0.001 5 eV) and an ultrabroad tuning range (0.47 eV), leading to a very large tuning range to bandwidth ratio. Such a device may find various applications including non-dispersive infrared sensing. When applied to NDIR sensing, such emitters can eliminate the need of filters[40] or specially designed spectral selective IR detectors,[5] leading to a scheme of multiplexed NDIR gas sensing that is simple, compact, and cost-effective.

This work was supported by a U. S. Army Research Office (ARO) MURI research grant (No. W911NF-19-1-0279) and by a grant from the U. S. Department of Energy (Grant No. DE-FG02-07ER46426).

DATA AVAILABILITY

The data that support the findings of this study are available from the corresponding author upon reasonable request.

REFERENCES

[1]S. Fan, "Thermal photonics and energy applications," Joule **1**, 264–273 (2017).
[2]W. Li and S. Fan, "Nanophotonic control of thermal radiation for energy applications [Invited]," Opt. Express **26**, 15995–16021 (2018).
[3]J. Hodgkinson and R. P. Tatam, "Optical gas sensing: A review," Meas. Sci. Technol. **24**, 012004 (2013).
[4]D. Jung, S. Bank, M. L. Lee, and D. Wasserman, "Next-generation mid-infrared sources," J. Opt. **19**, 123001 (2017).
[5]X. Tan, H. Zhang, J. Li, H. Wan, Q. Guo, H. Zhu, H. Liu, and F. Yi, "Non-dispersive infrared multi-gas sensing via nanoantenna integrated narrowband detectors," Nat. Commun. **11**, 5245 (2020).
[6]L. J. Jiang, E. Y. K. Ng, A. C. B. Yeo, S. Wu, F. Pan, W. Y. Yau, J. H. Chen, and Y. Yang, "A perspective on medical infrared imaging," J. Med. Eng. Technol. **29**, 257–267 (2005).
[7]K. Du, Q. Li, W. Zhang, Y. Yang, and M. Qiu, "Wavelength and thermal distribution selectable microbolometers based on metamaterial absorbers," IEEE Photonics J. **7**, 1–8 (2015).
[8]X. L. Liu, L. P. Wang, and Z. M. Zhang, "Wideband tunable omnidirectional infrared absorbers based on doped-silicon nanowire arrays," J. Heat Transfer **135**, 061602 (2013).
[9]Q. Tan, L. Tang, M. Yang, C. Xue, W. Zhang, J. Liu, and J. Xiong, "Three-gas detection system with IR optical sensor based on NDIR technology," Opt. Lasers Eng. **74**, 103–108 (2015).
[10]M. Dong, C. Zheng, S. Miao, Y. Zhang, Q. Du, Y. Wang, and F. K. Tittel, "Development and measurements of a mid-infrared multi-gas sensor system for CO, CO_2 and CH_4 detection," Sensors **17**, 2221 (2017).
[11]T. Inoue, M. D. Zoysa, T. Asano, and S. Noda, "Wavelength-switchable mid-infrared narrowband thermal emitters based on quantum wells and photonic crystals," IEICE Trans. Electron. **E101.C**, 545–552 (2018).
[12]X. Liu and W. J. Padilla, "Dynamic manipulation of infrared radiation with MEMS metamaterials," Adv. Opt. Mater. **1**, 559–562 (2013).
[13]M. A. Kats, R. Blanchard, S. Zhang, P. Genevet, C. Ko, S. Ramanathan, and F. Capasso, "Vanadium dioxide as a natural disordered metamaterial: Perfect thermal emission and large broadband negative differential thermal emittance," Phys. Rev. X **3**, 041004 (2013).
[14]T. Inoue, M. D. Zoysa, T. Asano, and S. Noda, "Realization of dynamic thermal emission control," Nat. Mater. **13**, 928–931 (2014).
[15]T. Inoue, M. De Zoysa, T. Asano, and S. Noda, "On-chip integration and high-speed switching of multi-wavelength narrowband thermal emitters," Appl. Phys. Lett. **108**, 091101 (2016).
[16]K.-K. Du, Q. Li, Y.-B. Lyu, J.-C. Ding, Y. Lu, Z.-Y. Cheng, and M. Qiu, "Control over emissivity of zero-static-power thermal emitters based on phase-changing material GST," Light: Sci. Appl. **6**, e16194 (2017).
[17]J. Park, J.-H. Kang, X. Liu, S. J. Maddox, K. Tang, P. C. McIntyre, S. R. Bank, and M. L. Brongersma, "Dynamic thermal emission control with InAs-based plasmonic metasurfaces," Sci. Adv. **4**, eaat3163 (2018).
[18]A. K. Moridani, R. Zando, W. Xie, I. Howell, J. J. Watkins, and J.-H. Lee, "Plasmonic thermal emitters for dynamically tunable infrared radiation," Adv. Opt. Mater. **5**, 1600993 (2017).
[19]D. D. Kang, T. Inoue, T. Asano, and S. Noda, "Electrical modulation of narrow-band GaN/AlGaN quantum-well photonic crystal thermal emitters in mid-wavelength infrared," ACS Photonics **6**, 1565–1571 (2019).
[20]K. Du, L. Cai, H. Luo, Y. Lu, J. Tian, Y. Qu, P. Ghosh, Y. Lyu, Z. Cheng, M. Qiu, and Q. Li, "Wavelength-tunable mid-infrared thermal emitters with a non-volatile phase changing material," Nanoscale **10**, 4415–4420 (2018).
[21]H. Zhu, H. Luo, Q. Li, D. Zhao, L. Cai, K. Du, Z. Xu, P. Ghosh, and M. Qiu, "Tunable narrowband mid-infrared thermal emitter with a bilayer cavity enhanced Tamm plasmon," Opt. Lett. **43**, 5230–5233 (2018).
[22]Z. Wang, J. K. Clark, Y.-L. Ho, S. Volz, H. Daiguji, and J.-J. Delaunay, "Ultranarrow and wavelength-tunable thermal emission in a hybrid metal–optical tamm state structure," ACS Photonics **7**, 1569–1576 (2020).
[23]J. Briere, M. Elsayed, M. Saidani, M. Bérard, P.-O. Beaulieu, H. Rabbani-Haghighi, F. Nabki, and M. Ménard, "Rotating circular micro-platform with integrated waveguides and latching arm for reconfigurable integrated optics," Micromachines **8**, 354 (2017).
[24]Y. Guo and S. Fan, "Narrowband thermal emission from a uniform tungsten surface critically coupled with a photonic crystal guided resonance," Opt. Express **24**, 29896–29907 (2016).
[25]W. G. Spitzer, D. Kleinman, and D. Walsh, "Infrared properties of hexagonal silicon carbide," Phys. Rev. **113**, 127–132 (1959).
[26]S. Fan and J. D. Joannopoulos, "Analysis of guided resonances in photonic crystal slabs," Phys. Rev. B **65**, 235112 (2002).
[27]V. Liu and S. Fan, "S4: A free electromagnetic solver for layered periodic structures," Comput. Phys. Commun. **183**, 2233–2244 (2012).

[28]I. Amidror, *The Theory of the Moiré Phenomenon*, 2nd ed. (Kluwer Academic, Dordrecht, 2009).
[29]Z. Wu and Y. Zheng, "Moiré metamaterials and metasurfaces," Adv. Opt. Mater. **6**, 1701057 (2018).
[30]S. S. Sunku, G. X. Ni, B. Y. Jiang, H. Yoo, A. Sternbach, A. S. McLeod, T. Stauber, L. Xiong, T. Taniguchi, K. Watanabe, P. Kim, M. M. Fogler, and D. N. Basov, "Photonic crystals for nano-light in moiré graphene superlattices," Science **362**, 1153–1156 (2018).
[31]Q. Fu, P. Wang, C. Huang, Y. V. Kartashov, L. Torner, V. V. Konotop, and F. Ye, "Optical soliton formation controlled by angle twisting in photonic moiré lattices," Nat. Photonics **14**, 663–668 (2020).
[32]P. Wang, Y. Zheng, X. Chen, C. Huang, Y. V. Kartashov, L. Torner, V. V. Konotop, and F. Ye, "Localization and delocalization of light in photonic moiré lattices," Nature **577**, 42–46 (2020).
[33]G. Hu, Q. Ou, G. Si, Y. Wu, J. Wu, Z. Dai, A. Krasnok, Y. Mazor, Q. Zhang, Q. Bao, C.-W. Qiu, and A. Alù, "Topological polaritons and photonic magic angles in twisted α-MoO 3 bilayers," Nature **582**, 209–213 (2020).
[34]L. Zhu and S. Fan, "Near-complete violation of detailed balance in thermal radiation," Phys. Rev. B **90**, 220301 (2014).
[35]L. Zhu, Y. Guo, and S. Fan, "Theory of many-body radiative heat transfer without the constraint of reciprocity," Phys. Rev. B **97**, 094302 (2018).
[36]C. Guo and S. Fan, "Theoretical constraints on reciprocal and non-reciprocal many-body radiative heat transfer," Phys. Rev. B **102**, 085401 (2020).
[37]B. Zhao, C. Guo, C. A. C. Garcia, P. Narang, and S. Fan, "Axion-field-enabled nonreciprocal thermal radiation in Weyl semimetals," Nano Lett. **20**, 1923–1927 (2020).
[38]C. Guo, B. Zhao, D. Huang, and S. Fan, "Radiative thermal router based on tunable magnetic Weyl semimetals," ACS Photonics **7**, 3257–3263 (2020).
[39]Y. Tsurimaki, X. Qian, S. Pajovic, F. Han, M. Li, and G. Chen, "Large nonreciprocal absorption and emission of radiation in type-I Weyl semimetals with time reversal symmetry breaking," Phys. Rev. B **101**, 165426 (2020).
[40]T. Inoue, M. D. Zoysa, T. Asano, and S. Noda, "Filter-free nondispersive infrared sensing using narrow-bandwidth mid-infrared thermal emitters," Appl. Phys. Express **7**, 012103 (2014).